Spectroscopic factors from direct proton capture

C. Iliadis
Department of Physics and Astronomy, The University of North Carolina at Chapel Hill, Chapel Hill, North Carolina 27599-3255, USA
and Triangle Universities Nuclear Laboratory, Durham, North Carolina 27708-0308, USA

M. Wiescher
Department of Physics, University of Notre Dame, Notre Dame, Indiana 46556, USA
and Joint Institute for Nuclear Astrophysics, 210 Nieuwland Science Hall, University of Notre Dame, Notre Dame, Indiana 46556, USA
(Received 8 March 2004; published 3 June 2004)

Spectroscopic factors derived from direct capture studies are systematically compared to those obtained from transfer reaction experiments and from shell model calculations for the $A=16-32$ target mass region. The direct proton capture and proton transfer spectroscopic factors are obtained in the present work from a reanalysis of literature data by using the *same bound state potential parameters*. Our direct capture spectroscopic factors differ significantly from the values originally reported in the literature. The sensitivity of the direct capture cross section to different choices for the scattering potential is explored. We find evidence that spectroscopic factors obtained from direct capture studies are as reliable as those extracted from transfer measurements if the (direct capture) radial scattering wave function is calculated with a zero nuclear scattering potential instead of the common choice of a hard-sphere potential.

DOI: 10.1103/PhysRevC.69.064305 PACS number(s): 21.10.Jx

I. INTRODUCTION

According to the nuclear shell model, a spectroscopic factor depends on the overlap integral between the final state and the state formed by coupling the target state with the transferred particle to a coupled-channel state [1]. Spectroscopic factors obtained from experimental data provide important tests of shell-model wave functions since they are related to the occupation probabilities of individual single-particle orbits. Spectroscopic factors also represent one of the most important input information in the field of nuclear astrophysics. Both the nonresonant (i.e., direct capture) and the resonant contributions to thermonuclear reaction rates are directly proportional to the magnitude of spectroscopic factors [2].

The majority of spectroscopic factors have been measured in transfer reaction studies by using the distorted-wave Born approximation (DWBA) model of direct nuclear reactions [3]. The DWBA cross section is calculated from the distorted waves of the incoming and outgoing reaction channels, and from the bound state wave function of the transferred particle. In order to achieve agreement between theory and experimental data, the differential cross section is calculated for shell-model wave functions with various values of the transferred orbital angular momentum until the shape of the cross section is found to agree. The factor by which theory is multiplied to achieve agreement in magnitude provides the value of the spectroscopic factor for the final state. Uncertainties introduced by this method are related to the values of the optical model parameters to be employed, to the parameters determining the bound state radial wave function, and to contributions from multistep or compound-nucleus formation processes to the measured cross section. These difficulties are reflected especially in the older literature where different authors report very different values of spectroscopic factors for the same nuclear levels. More recent proton stripping reactions, however, have employed more reliable optical model parameters and were also performed at sufficiently high bombarding energies at which compound-nucleus formation is negligible. Consequently, spectroscopic factors from these experiments show much better agreement. One of the most extensive and reliable investigations of absolute spectroscopic factors derived from $(^3\mathrm{He},d)$ proton stripping reactions has been reported recently by Vernotte *et al.* [4].

Many authors do not report errors for spectroscopic factors measured with stripping reactions, mainly because of difficulties in quantifying the systematic effects mentioned earlier. Some authors adopted an error estimate which has been obtained from the comprehensive evaluation of measured single-particle spectroscopic factors in the $A=21-44$ mass region by Endt [5]. A comparison of spectroscopic factors for different reactions [e.g., $(^3\mathrm{He},d)$ and (d,n)] and for mirror states [e.g., $(^3\mathrm{He},d)$ and (d,p)] resulted in an experimental error of about 25% for individual measurements.

To a lesser extent, spectroscopic factors have also been measured in studies of direct proton capture. The method has been pioneered by Rolfs [6] and most direct capture experiments have been performed by the groups at Toronto [6–8], Münster [9–11], and Notre Dame [12,13]. A partial list of references is given in Table I. Direct capture has been described as a single-step process where the proton is directly captured, without formation of a compound nucleus, into a final bound state with the emission of a γ-ray. There are similarities between the processes of direct proton capture and proton stripping. For example, the measured cross sections for both processes are directly proportional to the spectroscopic factors of the final bound states. Furthermore, in both cases the theoretical cross sections, as well as the deduced spectroscopic factors, depend sensitively on the parameters of the potential used to calculate the bound state wave function. However, there is a difference, as pointed out

TABLE I. Some references to direct proton capture measurements. (Only studies involving target masses with $A \geq 16$ are listed.)

Reaction	Bound-state potential[a]	Bound state potential parameters[b]	Scattering potential	Ref.
$^{16}O(p,\gamma)^{17}F$	Square-well	$r_0=1.36$ fm	Hard-sphere	[6]
	Optical model[e]	[e]	Optical model[e]	[22]
$^{17}O(p,\gamma)^{18}F$	Square-well	$r_0=1.36$ fm	Hard-sphere	[6]
$^{18}O(p,\gamma)^{19}F$	Woods-Saxon[c]	$r_0=1.89$ fm, $a=0.7$ fm	Hard-sphere	[10]
$^{20}Ne(p,\gamma)^{21}Na$	Square-well	$r_0=1.36$ fm	Hard-sphere	[9]
$^{22}Ne(p,\gamma)^{23}Na$	Woods-Saxon	$r_0=1.63$ fm, $a=0.7$ fm	Hard-sphere	[11]
$^{24}Mg(p,\gamma)^{25}Al$	Square-well	$r_0=1.36$ fm	Hard-sphere	[8]
$^{27}Al(p,\gamma)^{28}Si$	Woods-Saxon	$r_0=1.25$ fm, $a=0.65$ fm	Woods-Saxon[d]	[21]
$^{28}Si(p,\gamma)^{29}P$	Woods-Saxon	$r_0=1.25$ fm, $a=0.65$ fm	Hard-sphere	[12]
	Square-well	$r_0=1.35$ fm	Hard-sphere	[16]
$^{32}S(p,\gamma)^{33}Cl$	Woods-Saxon	$r_0=1.25$ fm, $a=0.65$ fm	Hard-sphere	[13]
$^{40}Ca(p,\gamma)^{41}Sc$	Square-well	$r_0=1.35$ fm	Hard-sphere	[17]

[a]Potential used for the calculation of the bound state wave function.
[b]Parameters of the bound state potential; the relationship of the nuclear radius R and the radius parameter r_0 is given by $R=r_0(A_t^{1/3}+A_p^{1/3})$ for a square-will potential, and by $R=r_0A_t^{1/3}$ for a Woods-Saxon potential; a is the diffuseness parameter for the Woods-Saxon potential; the potential depth is adjusted to reproduce the binding energy of the bound state.
[c]A square-well potential with $r_0=1.35$ fm has also been used in Ref. [10].
[d]With a potential depth of 55.14 MeV and parameters of $r_0=1.25$ fm and $a=0.65$ fm.
[e]Bound state and scattering state wave functions generated with the same optical model potential.

by Ref. [6]. Direct proton capture is induced by the relatively weak and well-known electromagnetic interaction, while proton stripping proceeds via the stronger and less well-known nuclear force. For this reason, some authors have suggested that direct capture studies may yield more reliable spectroscopic factors compared to those deduced from proton transfer reactions. On the other hand, the direct capture method has a certain disadvantage compared to the DWBA procedure, which is rarely appreciated in the literature. While most recent proton-stripping studies were performed at sufficiently high bombarding energies in order to minimize cross section contributions from compound-nucleus formation, such a choice is usually not possible in studies of direct proton capture which are typically performed in the presence of strong (and sometimes overlapping) broad resonances. Evidently, the larger the resonance contribution to the total cross section, the more difficult the determination of the direct capture amplitude will be.

It is interesting to note that in his evaluation, Endt [5] remarks that, as yet, it is difficult to judge the reliability of extracting spectroscopic factors from direct proton capture experiments. He also notes that for the reactions $^{20}Ne+p$ and $^{24}Mg+p$ proton transfer and direct capture measurements yield consistent results, while for $^{22}Ne+p$ the direct capture spectroscopic factors seem to be far too large. Surprisingly, a systematic investigation of direct capture spectroscopic factors is lacking so far.

It is our goal to investigate the reliability of the direct capture method for determining spectroscopic factors. We have reanalyzed available literature data from proton stripping reactions and from direct capture studies on *sd*-shell target nuclei, and have extracted spectroscopic factors by using the *same bound state potential parameters* in both cases. The quantitative comparison of spectroscopic factors derived from direct capture experiments to those from DWBA studies and to shell model results represents a sensitive test of the direct capture method. We also investigate the influence of the scattering potential on the value of the derived direct capture spectroscopic factors. It will be shown that previous direct capture model studies, which have neglected the contribution of the nuclear interior to the transition probability, frequently overestimate spectroscopic factors. Our results have implications beyond the field of nuclear structure since nonresonant and resonant contributions to thermonuclear reaction rates are directly proportional to spectroscopic factors [2].

We are considering in the present work spectroscopic factors rather than asymptotic normalization coefficients (ANCs). The former quantities are predominantly determined by the behavior of the radial overlap function inside the nucleus. The latter quantities are inherently less sensitive to the parameters used for describing the bound-state potential (see Ref. [14], and references therein). We adopted the spectroscopic factor description for ease of comparison with previous results. We emphasize that spectroscopic factors and asymptotic normalization coefficients represent only intermediate steps in calculating the quantities of interest in nuclear physics or nuclear astrophysics, such as cross sections or partial widths. The latter quantities are rather insensitive to the parameters of the bound-state potential and, therefore, both descriptions (using either spectroscopic factors or ANCs) should yield similar results. This issue has

been discussed in detail in the $^{14}N+p\rightarrow{}^{15}O$ study by Bertone *et al.* [15] who indeed find[1] that very similar values (and uncertainties) for cross sections and partial widths are obtained by using either description.

In Sec. II we present the input data and describe our procedure in detail. Results are discussed in Sec. III and a summary is given in Sec. IV. Throughout this work, all quantities are given in the laboratory system unless mentioned otherwise.

II. PROCEDURE

A. General considerations

In almost all direct capture studies listed in Table I, the authors compare their derived spectroscopic factors to those obtained from previous proton stripping reactions. Typically, all available transfer results are compiled which usually scatter over a large range of values. As a consequence, in almost all direct capture studies, the authors note "agreement" with results from transfer reactions and conclude that the direct capture method works rather well. It is important for the reader to realize that this comparison of spectroscopic factors has serious flaws for several reasons.

First, it can be seen from Table I that some direct capture studies [6,8,9,16,17] have used a square-well potential for the calculation of the bound state wave function. However, it is not appropriate to compare these direct capture spectroscopic factors with those from transfer reaction studies which are usually obtained by using a Woods-Saxon potential for the calculation of the bound state wave function. Second, it is also apparent from Table I that some authors [10,11] adopted very large values for the radius parameter of the Woods-Saxon bound state potential ($r_0=1.57-1.89$ fm). No justification is provided for choosing such large values. Clearly, it is not appropriate to compare, for example, a direct capture spectroscopic factor obtained with a Woods-Saxon bound state potential radius parameter of $r_0=1.8$ fm with the corresponding DWBA value obtained with a radius parameter of $r_0=1.25$ fm. Third, direct capture spectroscopic factors should be compared only to more recent transfer results since those values, as already mentioned in Sec. I, have been obtained with improved optical model parameters at higher bombarding energies, where compound-nucleus formation is negligible.

It is clear from the earlier discussion that the values of spectroscopic factors from direct proton capture studies and from proton transfer reactions, as reported in the literature, cannot be compared directly. Rather, the available cross section data from both types of experiments have to be reanalyzed using the *same potential parameters* for the calculation of the bound state radial wave function. (See also the discussion in Ref. [14].)

[1]From Fig. 5 in Ref. [15] it can be seen that the average standard deviation for the ground state S-factor amounts to 12% if ANCs are used in the data analysis. The corresponding number obtained by using spectroscopic factors is 20%. The ground state transition represents a worst-case scenario since these differences diminish quickly with decreasing binding energy.

In order to avoid confusion with the astrophysical S factor, we will discuss and compare in the following the quantity C^2S rather than the spectroscopic factor itself. The square of the isospin Clebsch-Gordan coefficient [1] for direct capture and proton transfer is given by $C^2=1$ for ^{16}O, ^{24}Mg, ^{28}Si, ^{32}S target nuclei, by $C^2=1/2$ for the target nucleus ^{17}O, and by $C^2=2/3$ or $1/3$ for the target nucleus ^{18}O (for $T=1/2$ or $3/2$ final states, respectively).

B. Selection of data

Any meaningful comparison of spectroscopic factors should be based only on published results which are subject to insignificant systematic errors. Since there is always a danger of selecting a biased data set (e.g., an incorrectly measured cross section), we will describe our selection strategy in more detail.

We started by compiling from the literature all nuclear levels for which spectroscopic factors from direct capture experiments as well as from proton transfer studies are available. In a second step, we disregarded those levels for which less reliable spectroscopic factors have been reported, including transitions to unbound states and to unresolved doublets. Transitions involving orbital angular momentum mixtures have been excluded as well, since in such cases the extraction of different orbital angular momentum components from the measured angular distributions introduces an additional source of uncertainty. We did not consider further older proton transfer studies which were performed at bombarding energies below $E_b=15$ MeV. Some older studies were mostly concerned with relative values of spectroscopic factors and have employed less reliable optical model parameters. We removed those cases as well. The resulting truncated data set was then *evaluated* as discussed in the following subsections. In a final step, we compiled from the literature theoretical spectroscopic factors which were obtained from shell model calculations.

Several more levels have been disregarded in the present work although they passed the selection criteria mentioned earlier. These cases are discussed in more detail in the Appendix.

C. Direct capture

1. Capture reaction measurements

It is important to recall how the results from direct proton capture studies, listed in Table I, have been analyzed. The experiments are usually performed by measuring the (p,γ) excitation function over an extended bombarding energy range, say, between $E_p=1$ and 3 MeV. For most radiative capture reactions, the measured excitation function (i.e., the yield versus bombarding energy) consists of several more or less pronounced resonances which are superimposed on a slowly varying "nonresonant background" contribution and the problem arises of how to interpret the data. Most authors, following the procedure suggested by Rolfs and Azuma [7], analyze the excitation function for a specific γ-ray transition in terms of a coherent sum of contributions from resonances and the direct capture process. At this point, it is sufficient to

TABLE II. Information from direct capture studies.

E_x[a] (keV)	$J^\pi; T$[a]	E_p^{labb} (keV)	$\sigma_{DC,exp}^{lit}$[c] (μb)	$n\ell_f$[d]	C^2S_{DC} previous[e]
		$^{16}O(p,\gamma)^{17}F$ (Q=600 keV)			
0	$5/2^+$	1369	0.69±0.08[f]	1d	
495	$1/2^+$	1369	2.83±0.08[f]	2s	
		$^{17}O(p,\gamma)^{18}F$[g] (Q=5607 keV)			
0	1^+	1625	0.37±0.08[h]	1d	0.50[h]
1042	$0^+;1$	1625	0.16±0.04[h]	1d	0.78[h]
1121	5^+	1625	1.74±0.34[h]	1d	0.78[h]
3358	3^+	1625	0.21±0.06[h]	2s	0.04[h]
4360	1^+	1625	0.02±0.01[h]	1d	0.11[h]
4652	$4^+;1$	1625	0.39±0.09[h]	1d	0.77[h]
		$^{18}O(p,\gamma)^{19}F$ (Q=7994 keV)			
0	$1/2^+$	1850	8.4±1.1[i]	2s	0.52±0.07[i]
197	$5/2^+$	1850	6.2±1.3[i]	1d	0.70±0.14[i]
1554	$3/2^+$	1850	2.3±0.5[i]	1d	0.45±0.11[i]
		$^{24}Mg(p,\gamma)^{25}Al$ (Q=2271 keV)			
0	$5/2^+$	823	0.008±0.002[j]	1d	0.10±0.03[j]
452	$1/2^+$	823	0.052±0.011[j]	2s	0.43±0.09[j]
945	$3/2^+$	823	0.004±0.001[j]	1d	0.11±0.03[j]
		$^{32}S(p,\gamma)^{33}Cl$ (Q=2277 keV)			
0	$3/2^+$	1378	0.033±0.008[k]	1d	0.84±0.21[k]
811	$1/2^+$	1378	0.048±0.009[k]	2s	0.28±0.05[k]

[a]Excitation energies and quantum numbers adopted from Refs. [40–42].
[b]Bombarding energy at which cross section for direct capture (column 4) is determined.
[c]Previously measured direct capture cross sections.
[d]Assumed $n\ell_f$ transfer.
[e]Previously reported C^2S_{DC} values; the quoted uncertainties represent errors in absolute experimental cross sections only.
[f]From Table IV of Ref. [22].
[g]Only pure transitions (i.e., those with a single value of ℓ_f) considered.
[h]From Tables II and III of Ref. [6].
[i]From Table 7 of Ref. [10].
[j]From Table I of Ref. [8].
[k]From Ref. [43] and Table III of Ref. [13].

note that in these studies the resonances are described by Breit-Wigner expressions [18] with energy-dependent partial widths, while the direct capture contribution is calculated by assuming that the nuclear interior does not contribute to the transition amplitude, i.e., the capture is strictly treated as an "extranuclear" process. We will come back to the latter issue in Sec. II C 4.

In Table II we list in the first four columns the excitation energy of final bound states, their quantum numbers, the bombarding energy at which the direct capture cross section has been measured, and the value of the extracted experimental direct capture cross section as reported in the literature.

2. Direct capture model

After extraction of the direct capture cross section from the measured excitation function, the spectroscopic factor can in principle be obtained. If the direct capture process proceeds to only one single-particle orbit of principle quantum number n and orbital angular momentum ℓ_f, then the spectroscopic factor is given by the expression

$$\sigma_{\mathrm{DC,exp}} = C^2 S(n,\ell_f) \sum_{\ell_i} \sigma_{\mathrm{DC,calc}}(n,\ell_i,\ell_f), \tag{1}$$

where $\sigma_{\mathrm{DC,exp}}$ and $\sigma_{\mathrm{DC,calc}}$ denote the measured and the calculated direct capture cross section, respectively. The sum in Eq. (1) is over all values of orbital angular momenta ℓ_i of the (initial) scattering wave function.

The quantity $\sigma_{\mathrm{DC,calc}}$ is calculated by using a single-particle potential model (for an interesting discussion, see Refs. [19,20]). The dominant E1 contribution to the (p,γ) cross section (in μb) for capture from an initial scattering state to a final bound state with orbital angular momenta of ℓ_i and ℓ_f, respectively, is given by [6]

$$\sigma_{\mathrm{DC,calc}}(E1) = 0.0716 \mu^{\frac{3}{2}} \left(\frac{Z_p}{A_p} - \frac{Z_t}{A_t} \right)^2 \times \frac{E_\gamma^3}{E^{\frac{3}{2}}} \frac{(2J_f+1)(2\ell_i+1)}{(2j_p+1)(2j_t+1)(2\ell_f+1)} \times (\ell_i 010|\ell_f 0)^2 R^2_{n\ell_i 1\ell_f}, \tag{2}$$

$$R_{n\ell_i 1\ell_f} = \int_0^\infty u_c(r) O_{E1}(r) u_b(r) r^2 dr, \tag{3}$$

with Z_i and A_i as the charges and masses (in amu) of projectile and target; j_p, j_t, J_f as the spins of projectile, target, and final state, respectively; E and E_γ as the bombarding proton energy and the energy of the γ-ray transition, respectively; O_{E1} as the radial part of the $E1$ multipole operator; u_c and u_b as the radial wave functions of the initial scattering state and final bound state, respectively.

3. Bound state potential

In the present work, the bound-state wave function, u_b, is generated by using a potential consisting of a Woods-Saxon term and a Coulomb term

$$V(r) = V_{\mathrm{WS}}(r) + V_C(r) = \frac{-V_0}{1 + e^{\frac{r-R}{a}}} + V_C(r), \tag{4}$$

with $R = r_0 A_t^{1/3}$, $r_0 = 1.25$ fm, and $a = 0.65$ fm; V_C corresponds to a uniformly charged sphere of radius $R_C = r_C A_t^{1/3}$ with $r_C = 1.25$ fm. The well depths V_0 were chosen to reproduce the binding energies of the final states so that the wave function has the correct asymptotic behavior.

As already mentioned in Sec. II A, for a number of capture reactions (see Table I) square-well potentials have been used previously in the calculation of bound state wave functions. For example, in the analysis of $^{16}\mathrm{O}+p$ and $^{17}\mathrm{O}+p$ capture data Rolfs [6] used a value of $R = 1.36(A_t^{1/3} + A_p^{1/3})$ fm for the radius of the square-well potential. The same radius parameter of $r_0 = 1.36$ fm was adopted in subsequent capture studies on ^{20}Ne, ^{24}Mg, ^{28}Si, and ^{40}Ca target nuclei [8,9,16,17], although no justification for this particular choice was provided by these authors. In order to investigate this issue further we display in Fig. 1 radial bound state wave functions for the levels at $E_x = 3358$ and 4652 keV in ^{18}F. The solid and dashed lines correspond to results obtained by using a Woods-Saxon potential ($r_0 = 1.25$ fm, $a = 0.65$ fm) and a square-well potential ($r_0 = 1.36$ fm), respectively. In both cases, the potential depths are adjusted to reproduce the experimental binding energy.

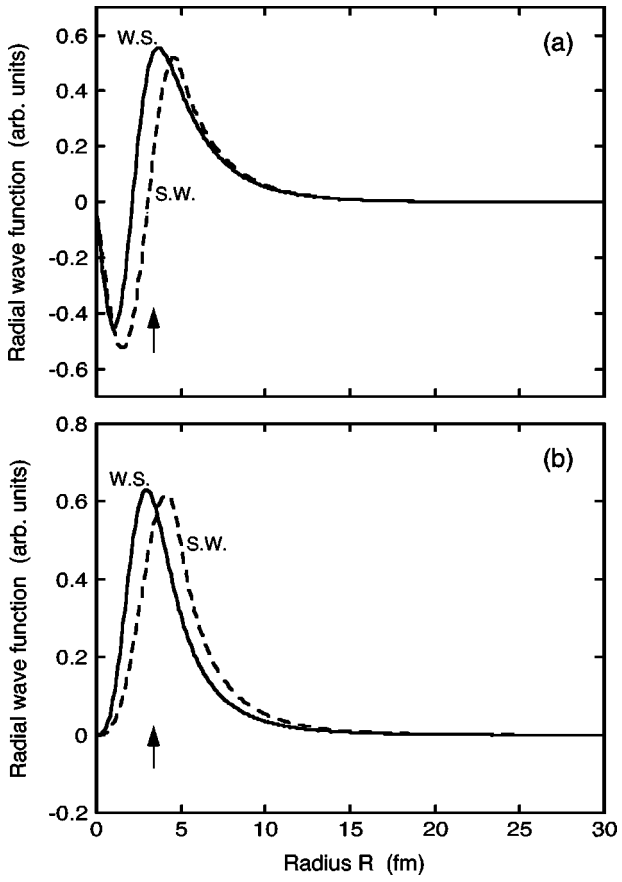

FIG. 1. Bound state radial wave functions for the levels at (a) $E_x = 3358$ keV ($2s$) and (b) 4652 keV ($1d$) in ^{18}F. The solid lines are obtained with a Woods-Saxon potential ($r_0 = 1.25$ fm, $a = 0.65$ fm) while the dashed lines are calculated for a square-well potential ($r_0 = 1.36$ fm). The potential depths are $V_0 = 57.2$ MeV ($E_x = 3358$ keV, Woods-Saxon potential), 28.7 MeV ($E_x = 3358$ keV, square-well potential), 56.0 MeV ($E_x = 4652$ keV, Woods-Saxon potential) and 23.1 MeV ($E_x = 4652$ keV, square-well potential). The arrows indicate the radius R of the Woods-Saxon potential.

Figure 1(a) shows the radial bound state wave functions for the level at $E_x = 3358$ keV, representing capture into a $2s$ single-particle orbit. It can be seen that the bound state wave functions differ substantially inside and near the nuclear radius. However, the tails of the radial bound state wave functions outside the nucleus are in close agreement. Therefore, the calculated direct capture cross sections and corresponding spectroscopic factors for the $^{17}\mathrm{O}+p$ reaction will also be in agreement if it is assumed that the nuclear interior does not contribute to the transition amplitude (i.e., if a hard-sphere potential is used for the calculation of the scattering wave function; the latter assumption was applied in most previous studies, see Table I). Similar conclusions hold for other states considered in the present work which are represented by $2s$ single-particle orbits.

In Fig. 1(b) we show the radial bound state wave functions for the level at $E_x = 4652$ keV, assuming capture into a $1d$ single-particle orbit. It is evident that the two bound state radial wave functions differ not only inside the nucleus, but outside the nuclear radius as well. Even if it is assumed that the nuclear interior does not contribute to the transition amplitude, we expect in this case significant differences in the calculated cross section as well as for the corresponding spectroscopic factors. Similar conclusions hold for other levels of interest in the present work which are represented by $1d$ single-particle orbits.

4. Scattering potential

The scattering wave function u_c, which can be generated with a suitable scattering potential, is the only remaining quantity needed for the calculation of the direct capture cross section $\sigma_{\mathrm{DC,calc}}$ [see Eqs. (2) and (3)]. We will now discuss this issue in more detail. Consider a proton approaching a target nucleus at very low bombarding energy so that the de Broglie wavelength of the incident particle is large compared to the nuclear radius. Suppose further that the proton is captured into a state of low binding energy, implying that the bound state wave function will extend substantially beyond the nuclear radius. As one approaches the nuclear surface, the amplitude of the scattering wave function decreases and becomes negligible inside the nucleus, while at the same time the exterior part of the bound state wave function increases. The product of both wave functions [see Eq. (3)] will then have a maximum outside the nuclear surface. The calculated cross section is rather insensitive to the details of the model used for the nuclear interior and, therefore, the direct capture process is sometimes referred to as extranuclear capture. While we expect this particular property to hold at low bombarding energies *and* for levels of small binding energy, the contribution of the nuclear interior to the transition amplitude may not be negligible anymore either at higher bombarding energies (i.e., where most direct capture cross sections have been measured; see column 3 in Table II) or for strongly bound levels. Consequently, the direct capture cross section could depend sensitively on the nuclear potential used to generate the scattering wave function.

In the past, different authors have approached this problem in different ways. As can be seen from Table I, most of the previous studies have assumed hard-sphere scattering potentials, thereby treating the direct capture process strictly as extranuclear capture, as pointed out earlier. Some authors used optical model potentials and adjusted the potential parameters to reproduce elastic scattering observables. However, for the target mass range of interest in the present work, this approach is only possible in exceptional cases (for example, $^{16}\mathrm{O}+p$). In fact, for most target nuclei listed in Table I, the nuclear scattering phase shifts have not been measured below $E_p = 2$ MeV since the elastic scattering process at those energies is entirely dominated by Coulomb scattering. Other authors [21] prefered to use global optical model potentials. Finally, in some studies (see Ref. [22–25]) the scattering state wave function was generated with the same potential that was used to calculate the bound state wave function.

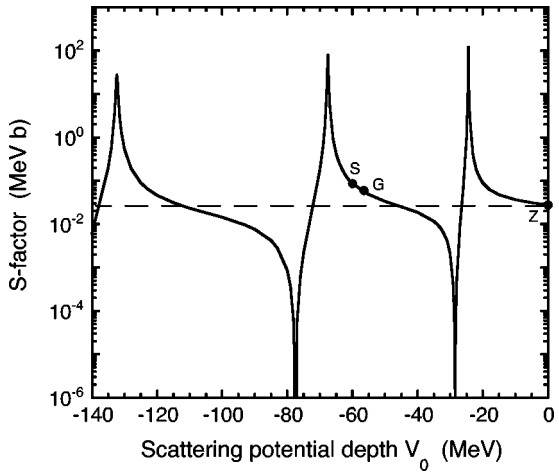

FIG. 2. Calculated S factor for the $^{22}\mathrm{Ne}(p,\gamma)^{23}\mathrm{Na}$ reaction populating the $E_x = 2391$ keV state versus scattering potential depth. The bombarding energy is held constant at $E_p = 1220$ keV. The S factor varies by several orders of magnitude and exhibits three resonances. The full circles labeled "S," "G," and "Z" correspond to different choices of potential depths. Note, that the dashed line, corresponding to the S factor obtained with a nuclear scattering potential of zero, intersects the solid curve at the inflection points between the resonances.

In Fig. 2 we display the S factor, calculated according to Eqs. (2) and (3), for the $^{22}\mathrm{Ne}+p$ reaction (at a bombarding energy of $E_p = 1220$ keV and for a $^{23}\mathrm{Na}$ excitation energy of $E_x = 2391$ keV) versus the depth of the Woods-Saxon potential used to generate the scattering wave function. It can be seen that the S factor varies by several orders of magnitude and exhibits three resonances, corresponding to no node, one node and two nodes, respectively, of the scattering wave function in the region of the nucleus. If, for some reason, the scattering potential depth chosen gives rise to a resonance, then the values for both the calculated "direct capture" cross section and the deduced spectroscopic factor [Eq. (1)] will be erroneous. The obvious conclusion one can draw from Fig. 2 is that *the scattering potential has to be chosen carefully in order to calculate the non-resonant capture cross section.*

In the present work we adopt four different sets of nuclear potentials to calculate the scattering wave function u_c: (i) a hard-sphere potential of radius $R = 1.25A_t^{1/3}$ fm; (ii) a global optical model potential from Perey [26]; (iii) a bound state (Woods-Saxon) potential with a depth adjusted to reproduce the binding energy of the final state (Sec. II C 3); (iv) a potential of zero depth inside the radius of $R = 1.25A_t^{1/3}$ fm. These choices are labeled by "H," "G," "S," and "Z," respectively, in Figs. 2–6 that are discussed in the following.

In the following we explore the $^{22}\mathrm{Ne}+p$ reaction in more detail in order to better understand the dependence of the calculated S factor on the scattering potential. The results of calculations for two $^{23}\mathrm{Na}$ levels, a weakly bound state at $E_x = 8664$ keV and a strongly bound state at $E_x = 2391$ keV, are shown in Figs. 3–5. The corresponding S factors versus bombarding energy are shown in Fig. 3. The curves obtained for the different scattering potentials described earlier provide consistent results for the weakly bound $E_x = 8664$ keV state over the energy range of interest (e.g., at energies of

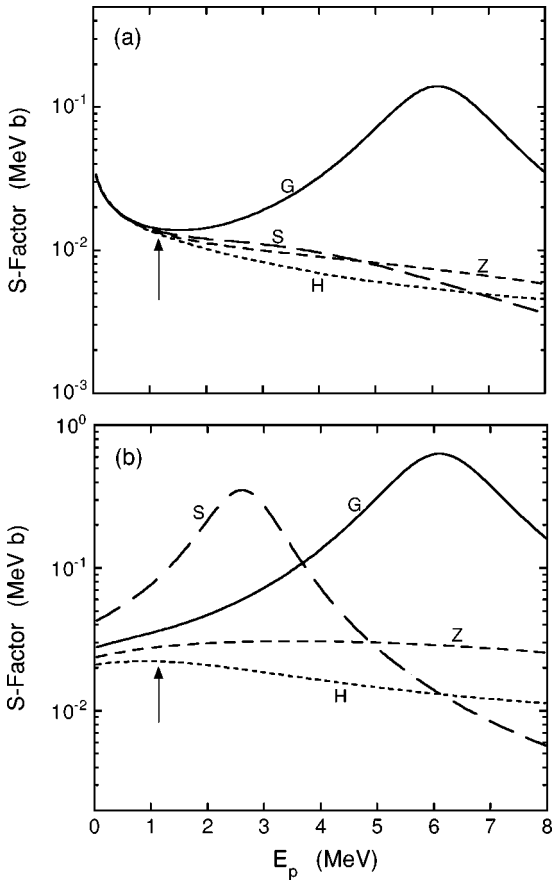

FIG. 3. Calculated S factor vs center-of-mass bombarding energy for the ^{22}Ne$(p,\gamma)^{23}$Na reaction populating the (a) E_x = 8664 keV state and the (b) E_x = 2391 keV state. The labels "H," "S," "G," and "Z" correspond to different choices of nuclear scattering potentials. The arrows indicate the energy at which the direct capture cross section has been measured [11].

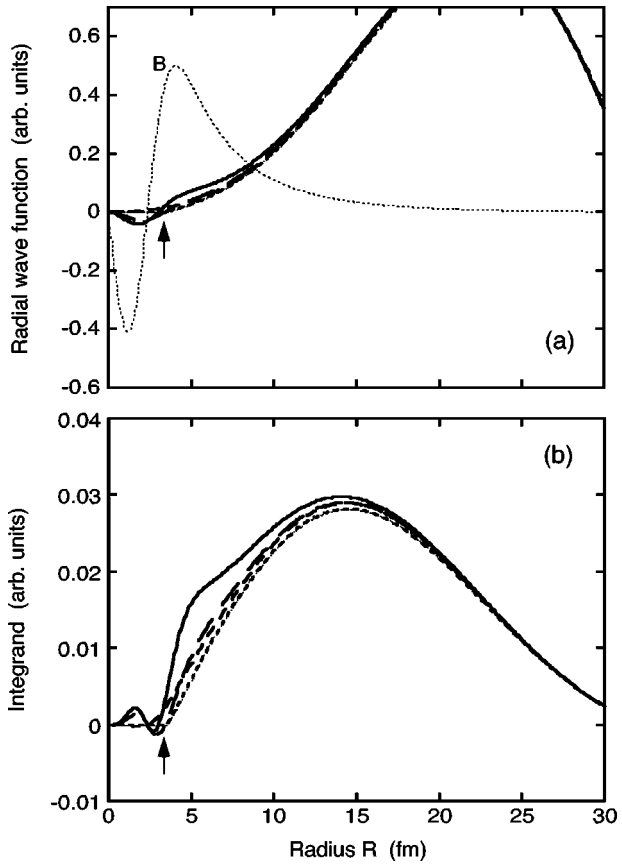

FIG. 4. (a) Radial wave functions and (b) the product $u_c(r)O_{E1}(r)u_b(r)r^2$ [i.e., the integrand in Eq. (3)], calculated at $E_p^{\rm cm}$ = 1167 keV for the ^{22}Ne$(p,\gamma)^{23}$Na reaction populating the E_x = 8664 keV state. In part (a), the dotted line labeled "B" shows the bound state radial wave function. The solid and dashed lines are obtained for different choices of the scattering potential (see text). The arrows indicate the nuclear radius $R = 1.25A_t^{1/3}$ fm.

E_p = 1–2 MeV at which the direct capture on ^{22}Ne has been measured [11], and at low energies $E_p \leqslant 200$ keV of astrophysical importance). However, for the strongly bound E_x = 2391 keV state certain scattering potentials give rise to resonances and the calculated S factor varies for different choices of V_0 (by a factor of 4 and 2 at energies of $E_p^{\rm lab}$ = 1220 keV and 0, respectively). The reason for the different S-factor dependence is shown in Figs. 4 and 5. The figures display the bound state radial wave functions, the scattering state radial wave functions, and the real part of the product $u_c(r)O_{E1}(r)u_b(r)r^2$ [i.e., the integrand in Eq. (3)], calculated at E_p = 1220 keV. For both ^{23}Na states the scattering wave functions shown in Figs. 4(a) and 5(a) are the same [except for choice (iv); see earlier]. However, the bound state wave functions reveal a crucial difference. For the weakly bound level at E_x = 8664 keV the bound state wave function extends far beyond the nuclear radius and the maximum of the integrand occurs at 15 fm [Fig. 4(b)]. Consequently, the contribution of the nuclear interior to the capture reaction is small and the S factor is relatively insensitive to the particular choice of the scattering potential. On the other hand, for the strongly bound level at E_x = 2391 keV the bound state wave function is more confined to the nuclear region [Fig. 5(a)] and the maximum of the integrand occurs at 5 fm [Fig. 5(b)]. In this case, the small differences in scattering wave functions close to the nuclear radius become much more important. Although the nuclear interior provides still only a small contribution to the capture reaction, it is obvious that the integrand, and hence the S factor, is much more sensitive to the choice of the scattering potential [Fig. 5(b)].

Direct capture spectroscopic factors, calculated according to Eqs. (1)–(3) by summing over contributions from different ℓ_i values, are listed in columns 3–6 of Table IV for the four different sets of scattering potentials. Previously reported direct capture spectroscopic factors are given in column 6 of Table II. The quoted errors include only the random uncertainties of the previously reported experimental cross sections (column 4 of Table II). They do not include systematic uncertainties introduced, for example, by our particular choice of bound or scattering state potential parameters. It is apparent from Tables II and IV that for many levels our $C^2S_{\rm DC}$ values differ significantly from those quoted in the original direct capture studies.

D. Transfer reactions

Transfer reactions are usually performed at a constant bombarding energy by measuring the angular distribution of

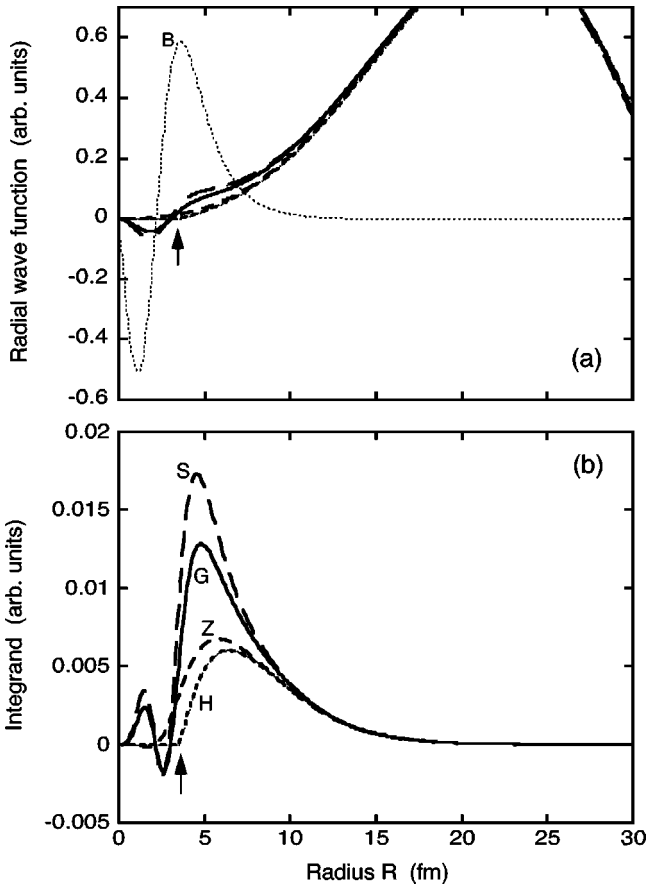

FIG. 5. Same as Fig. 4, but for the $E_x = 2391$ keV state.

the outgoing reaction products. For a transition which proceeds to only one single-particle orbit of principle quantum number n, orbital angular momentum ℓ_f, and total angular momentum j, the spectroscopic factor is given by the expression

$$\left(\frac{d\sigma}{d\Omega}\right)_{\rm exp} = N\frac{2J_f+1}{2j_t+1}\frac{1}{2j+1}\mathrm{C^2S}(n,\ell_f,j)\left(\frac{d\sigma_{n\ell_f j}}{d\Omega}\right)_{\rm DWBA}. \quad (5)$$

The normalization factor for proton stripping reactions is proportional to the square overlap integral between the wave functions of the ejectile coupled to the transferred proton and the projectile. The numerical value is given by $N=4.43$ for the $(^3\mathrm{He},d)$ reaction [27]. Most DWBA differential cross sections have been calculated in the past by using the code DWUCK4 [28]. In Table III we list in the first three columns the excitation energy of the final bound state, their quantum numbers, and the bombarding energy at which the differential transfer cross section has been measured. Literature values of measured spectroscopic factors are given in columns 4 and 5. More than half of those values are adopted from Ref. [4] which represents the most comprehensive $(^3\mathrm{He},d)$ transfer study available in the literature. We added to this data set the $(^3\mathrm{He},d)$ results of Refs. [29,30] for ^{18}F bound states. The errors listed in columns 4 and 5 of Table III include only the random uncertainties of the experimental cross sections as

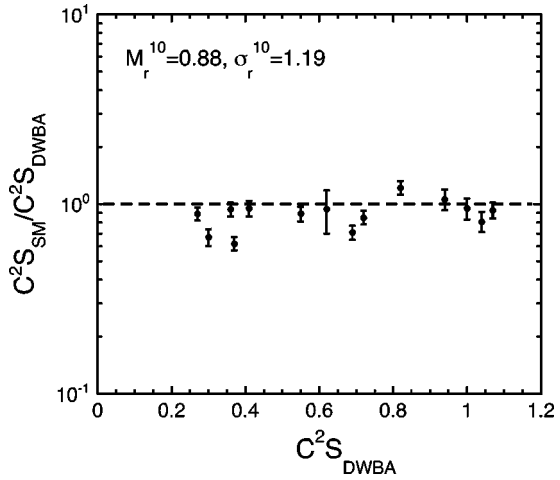

FIG. 6. Ratio of spectroscopic factors from shell model calculations (column 8 in Table IV (and from proton transfer studies (column 7 of Table IV). The displayed error bars include the uncertainties in the experimental proton transfer cross section only.

reported in the original literature. They do not include systematic uncertainties introduced by various assumptions of the DWBA model.

As pointed out in the introduction, a comparison of spectroscopic factors from direct capture and proton transfer is only meaningful if the same set of potential parameters is employed for the calculation of the bound state wave functions. Most transfer results listed in Table III have been obtained by using a bound state potential of Woods-Saxon shape, with the conventional parameters of $r_0=1.25$ fm and $a=0.65$ fm. It should also be noted that most of those studies used a spin-orbit term for the bound state potential (with a spin-orbit coupling of $\lambda=25$ times the Thomas term; see Table III). An extensive discussion of the influence of such a term on the numerical values of the extracted spectroscopic factors can be found in Ref. [4]. In the present work, we have reanalyzed for all levels listed in Table III the original transfer reaction data by using the bound state potential parameters of $r_0=1.25$ fm, $a=0.65$ fm, and $\lambda=0$, i.e., the same parameters as used for the calculations of the direct capture cross sections (Sec. II C 3). We performed these computations with the code DWUCK4. As usual, the depth of the bound state potential is chosen to reproduce the experimental binding energy. The distorted waves in the entrance and exit channels are generated with the same numerical values of the optical model potential parameters as used in the original papers. Our derived spectroscopic factors are listed in column 7 of Table IV. The present $\mathrm{C^2S_{DWBA}}$ values deviate from the original literature values (columns 4 and 5 of Table III) by 5%–33%.

E. Shell model

In column 8 of Table IV we list theoretical spectroscopic factors which were obtained from shell model calculations [4,31] in the complete $(1d_{5/2}2s_{1/2}1d_{3/2})$ model space. The

TABLE III. Information from transfer reaction studies.

E_x[a] (keV)	$J^\pi;T$[a]	E_b^{labb} (MeV)	C^2S_{DWBA}[c] previous	
		$^{16}O(^3He,d)^{17}F$ ($Q=-4893$ keV)		
0	$5/2^+$	25.0	1.00 ± 0.09[d]	
495	$1/2^+$	25.0	0.82 ± 0.07[d]	
		$^{17}O(^3He,d)^{18}F$ ($Q=113$ keV)		
0	1^+	15.0		0.62 ± 0.16[f]
1042	$0^+;1$	15.0	0.96 ± 0.14[e]	0.96 ± 0.24[f]
1121	5^+	15.0	0.89 ± 0.13[e]	0.83 ± 0.21[f]
3358	3^+	15.0	0.014 ± 0.002[e]	
4360	1^+	15.0	0.074 ± 0.011[e]	
4652	$4^+;1$	15.0	1.04 ± 0.16[e]	0.81 ± 0.20[f]
		$^{18}O(^3He,d)^{19}F$ ($Q=2501$ keV)		
0	$1/2^+$	25.0	0.41 ± 0.04[d]	
197	$5/2^+$	25.0	0.50 ± 0.05[d]	
1554	$3/2^+$	25.0	0.37 ± 0.03[d]	
		$^{24}Mg(^3He,d)^{25}Al$ ($Q=-3222$ keV)		
0	$5/2^+$	25.0	0.33 ± 0.03[d]	
452	$1/2^+$	25.0	0.69 ± 0.06[d]	
945	$3/2^+$	25.0	0.32 ± 0.03[d]	
		$^{32}S(^3He,d)^{33}Cl$ ($Q=-3217$ keV)		
0	$3/2^+$	25.0	0.86 ± 0.08[d]	
811	$1/2^+$	25.0	0.37 ± 0.03[d]	

[a]Excitation energies and quantum numbers adopted from Refs. [40–42].
[b]Bombarding energy at which transfer reaction has been studied.
[c]Previously reported C^2S_{DWBA} values; the quoted uncertainties represent errors in absolute experimental cross sections only.
[d]From Ref. [4] with an error of 6%–9% in the experimental absolute cross section; the bound state potential parameters used were $r_0=1.25$ fm, $a=0.65$ fm, and $\lambda=25$.
[e]From Ref. [29] with an error of 15% in the experimental absolute cross section; the bound state potential parameters used were $r_0=1.25$ fm, $a=0.65$ fm, and $\lambda=25$; a $1d_{5/2}$ transfer was assumed for all $\ell_f=2$ transitions.
[f]From Ref. [30] with an error of 25% in the experimental absolute cross section; the bound state potential parameters used were $r_0=1.25$ fm, $a=0.65$ fm, and $\lambda=0$.

shell model spectroscopic factors adopted from Ref. [4] were calculated by using the USD interaction [32], while those taken from Ref. [31] were computed with the $K+^{17}O$ interaction [33]. Both of these effective Hamiltonians conserve isospin. For the ^{19}F states listed in Table IV, spectroscopic factors calculated for both interactions are available from the literature and their values are in close agreement.

III. DISCUSSION OF RESULTS

A. Comparison of C^2S_{SM} with C^2S_{DWBA}

We start our discussion by comparing first spectroscopic factors measured in proton transfer reactions, C^2S_{DWBA}, with those calculated with the shell model, C^2S_{SM} (columns 7 and 8 in Table IV). In Fig. 6 we show the ratios C^2S_{SM}/C^2S_{DWBA} versus the value of C^2S_{DWBA}. Note, that the displayed error bars include the uncertainties in the experimental proton transfer cross sections only and that systematic uncertainties introduced by the DWBA reaction model have not been accounted for. It can be seen that the experimental C^2S_{DWBA} values are systematically larger compared to shell model results, although the deviation is small. In fact, the logarithmic[2] mean of the C^2S ratios amounts to $M_r^{10}=0.88$. The level of agreement is satisfactory considering that the two sets of C^2S values are obtained by entirely independent methods. It also follows that our choice of Woods-Saxon bound state potential parameters ($r_0=1.25$ fm and $a=0.65$ fm; Sec. II D) provides consistent C^2S_{DWBA} values. The logarithmic standard deviation of the ratio C^2S_{SM}/C^2S_{DWBA} amounts to $\sigma_r^{10}=1.19$. This result is in agreement with the 25% error (Sec. I) assigned to experimental C^2S_{DWBA} values by Endt's comprehensive evaluation [5]. We conclude from Fig. 6 that, for the levels under consideration here, the calculated shell model and measured proton transfer spectroscopic factors provide a consistent data set which is appropriate for testing the reliability of C^2S values obtained from direct capture studies.

B. Comparison of C^2S_{DC} with C^2S_{DWBA}

Ratios of spectroscopic factors obtained from direct capture and proton transfer measurements are shown in Figs. 7–10. The displayed error bars include only the random uncertainties of the two experimental cross sections (column 4 of Table II, and columns 4 and 5 of Table III).

In Fig. 7, the C^2S_{DC} values have been obtained from the measured direct capture cross sections [Eqs. (1)–(3)] by using hard-sphere scattering potentials (column 3 of Table IV). Recall, that this is the scattering potential of choice in the majority of direct capture studies (Table I). The logarithmic mean of the C^2S ratios amounts to $M_r^{10}=1.46$, indicating that the the C^2S_{DC} values are systematically larger than the values of C^2S_{DWBA}. According to Eq. (1), this deviation may be explained either by an overestimated experimental direct capture cross section (perhaps because of remaining resonant capture contributions that have not been subtracted from the total cross section) or by an underestimated calculated direct capture cross section (perhaps because the use of a hard-sphere potential disregards capture contributions from the region inside, and close to, the nuclear radius). The logarithmic standard deviation of the ratio C^2S_{DC}/C^2S_{DWBA} amounts to $\sigma_r^{10}=1.48$, a value that is close to the average error of the

[2]The logarithmic mean measures systematic trends, while the logarithmic standard deviation measures the scatter of the ratios around the logarithmic mean value; for a definition and explanation of these quantities, see Refs. [34,35].

TABLE IV. Comparison of spectroscopic factors.

E_x[a] (keV)	$J^\pi; T$[a]	C^2S					
		DC[b]	DC[c]	DC[d]	DC[e]	DWBA[f]	SM[g]
				$^{16}O+p\rightarrow{}^{17}F$			
0	$5/2^+$	1.2±0.1	1.2±0.1	1.1±0.1	1.1±0.1	1.07±0.10	1.0[h]
495	$1/2^+$	1.00±0.03	0.95±0.03	0.96±0.03	0.98±0.03	0.82±0.07	1.0[h]
				$^{17}O+p\rightarrow{}^{18}F$			
0	1^+	1.3±0.3	1.2±0.3	0.41±0.09	0.89±0.19	0.62±0.16	0.58[i]
1042	$0^+;1$	2.0±0.5	1.6±0.4	0.79±0.20	1.3±0.3	1.04±0.13	0.84[i]
1121	5^+	2.0±0.4	1.7±0.3	0.82±0.16	1.3±0.3	0.94±0.12	1.0[i]
3358	3^+	0.045±0.013	0.043±0.012	0.038±0.011	0.047±0.013	0.014±0.002	
4360	1^+	0.17±0.09	0.15±0.08	0.14±0.07	0.15±0.08	0.081±0.012	
4652	$4^+;1$	1.3±0.3	1.1±0.3	1.1±0.2	1.1±0.3	1.00±0.13	0.95[i]
				$^{18}O+p\rightarrow{}^{19}F$			
0	$1/2^+$	0.55±0.07	0.30±0.04	0.027±0.004	0.38±0.05	0.41±0.04	0.39[h]
197	$5/2^+$	0.98±0.21	0.64±0.13	0.075±0.016	0.53±0.11	0.55±0.05	0.49[h]
1554	$3/2^+$	0.62±0.13	0.40±0.09	0.11±0.02	0.35±0.08	0.30±0.03	0.20[h]
				$^{24}Mg+p\rightarrow{}^{25}Al$			
0	$5/2^+$	0.35±0.09	0.29±0.07	0.29±0.07	0.29±0.07	0.36±0.03	0.34[h]
452	$1/2^+$	0.58±0.12	0.52±0.11	0.51±0.11	0.56±0.12	0.69±0.06	0.49[h]
945	$3/2^+$	0.34±0.09	0.30±0.08	0.31±0.08	0.31±0.08	0.27±0.02	0.24[h]
				$^{32}S+p\rightarrow{}^{33}Cl$			
0	$3/2^+$	0.84±0.21	0.69±0.17	0.66±0.16	0.67±0.16	0.72±0.06	0.61[h]
811	$1/2^+$	0.26±0.05	0.24±0.05	0.22±0.04	0.25±0.05	0.37±0.03	0.23[h]

[a]Excitation energies and quantum numbers adopted from Refs. [40–42].
[b]From present work; obtained from column 4 of Table II by using a hard sphere scattering potential of radius $R=1.25A_t^{1/3}$ fm.
[c]From present work; obtained from column 4 of Table II by using a global optical model scattering potential from Ref. [26].
[d]From present work; obtained from column 4 of Table II by using for the scattering potential the same Woods-Saxon potential that is employed for calculating the bound state radial wave function.
[e]From present work; obtained from column 4 of Table II by using a nuclear scattering potential of zero depth inside the radius $R=1.25A_t^{1/3}$ fm.
[f]From present work; obtained from a reanalysis of literature data (listed in columns 4 and 5 of Table III) by using bound state potential parameters of $r_0=1.25$ fm, $a=0.65$ fm, and $\lambda=0$.
[g]From shell model calculations.
[h]From Table IV of Ref. [4].
[i]From Ref. [31].

displayed ratios. Hence, the scatter of the ratios C^2S_{DC}/C^2S_{DWBA} around the logarithmic mean value is consistent with the combined random errors of the experimental direct capture and proton transfer cross sections.

Results obtained with the global optical model scattering potential of Ref. [26] (column 4 of Table IV) instead of a hard-sphere potential for generating the (direct capture) scattering radial wave function are displayed in Fig. 8. The logarithmic mean of the C^2S ratios now amounts to $M_r^{10}=1.21$, representing a significant improvement compared to Fig. 7. These results support the conclusion that more reliable spectroscopic factors are obtained from measured direct capture cross sections if capture contributions inside, and close to, the nuclear radius are taken into account. The logarithmic standard deviation amounts to $\sigma_r^{10}=1.50$ and is similar to the value derived from Fig. 7.

Corresponding results obtained for a (direct capture) scattering potential that is identical to the one employed for the computation of the corresponding bound state radial wave function (column 5 of Table IV) are shown in Fig. 9. The

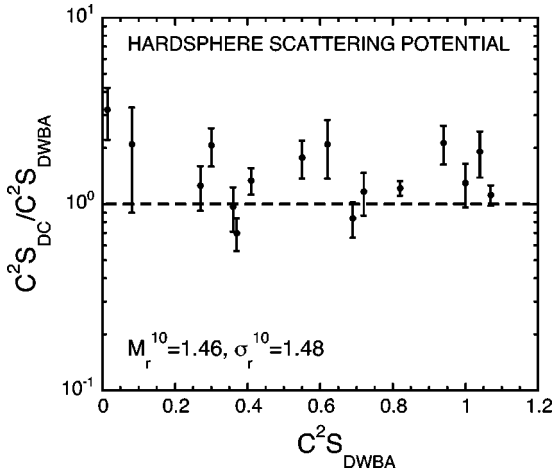

FIG. 7. Ratio of spectroscopic factors from direct capture (column 3 in Table IV) and from proton transfer studies (column 7 of Table IV). The direct capture data are obtained by using a hard-sphere scattering potential. The displayed error bars include the uncertainties in the experimental direct capture and proton transfer cross sections only.

logarithmic mean and standard deviation amount to $M_r^{10}=0.70$ and $\sigma_r^{10}=2.41$, respectively. It is evident that this choice of scattering potential yields far less reliable direct capture spectroscopic factors. (Note, that the data point for the ground state of ^{19}F is off scale.) The poor agreement reflects the sensitivity of the calculated direct capture cross section to the potential depth, an issue we already discussed in Sec. II C 4 in connection with Fig. 2. If the same potential is used for the calculation of bound state and scattering state radial wave functions, then the calculated cross section may in certain cases exhibit a resonant behavior. Since all resonant contributions have been supposedly subtracted from the measured total capture cross section, the direct capture spectroscopic factor obtained from Eq. (1) will be erroneous.

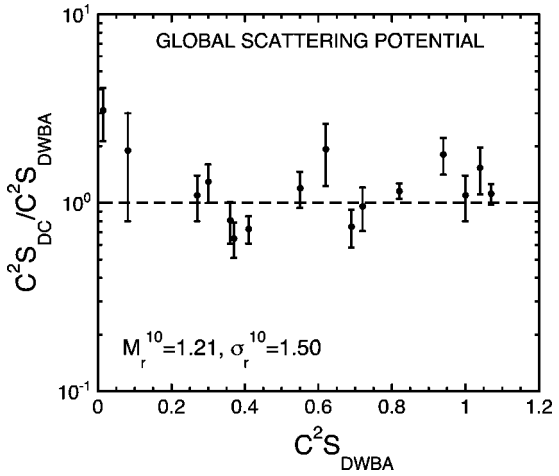

FIG. 8. Ratio of spectroscopic factors from direct capture (column 4 in Table IV) and from proton transfer studies (column 7 of Table IV). The direct capture data are obtained by using a global optical model scattering potential. The displayed error bars include the uncertainties in the experimental direct capture and proton transfer cross sections only.

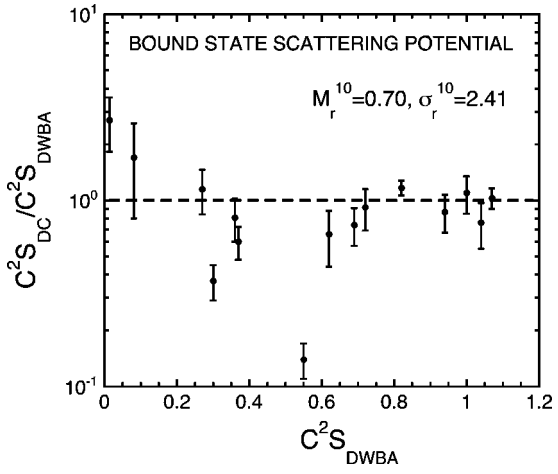

FIG. 9. Ratio of spectroscopic factors from direct capture (column 5 in Table IV) and from proton transfer studies (column 7 of Table IV). The direct capture data are obtained by using a scattering potential that is identical to the one employed for the computation of the corresponding bound state radial wave function. The displayed error bars include the uncertainties in the experimental direct capture and proton transfer cross sections only. Note, that the data point for the ground state of ^{19}F (see Table IV) is off scale.

Finally, we compare in Fig. 10 values of C^2S_{DC} and C^2S_{DWBA}, where the former are obtained by using a (direct capture) scattering potential depth of zero (column 6 of Table IV). The logarithmic mean and standard deviation of the ratio C^2S_{DC}/C^2S_{DWBA} amount to $M_r^{10}=1.15$ and $\sigma_r^{10}=1.44$, respectively. An inspection of Figs. 7–10 reveals that this choice of scattering potential provides the best overall agreement between spectroscopic factors from direct capture and proton transfer studies. This result can be understood by considering again, as an example, the S factor for the ^{22}Ne$(p\gamma)^{23}$Na reaction that is shown in Fig. 2. The dashed line, corresponding to the S factor obtained with a zero po-

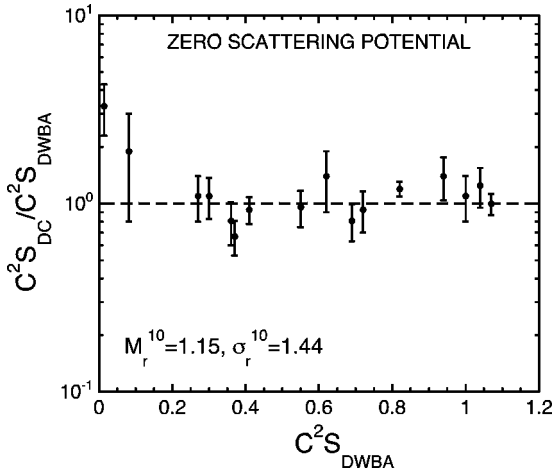

FIG. 10. Ratio of spectroscopic factors from direct capture (column 6 in Table IV) and from proton transfer studies (column 7 of Table IV). The direct capture data are obtained by using a nuclear scattering potential of zero depth. The displayed error bars include the uncertainties in the experimental direct capture and proton transfer cross sections only.

tential depth, intersects the solid line at the inflection points of the S-factor curve between the resonances, i.e., all the potential depths corresponding to these inflection points yield the same value for the S factor. It seems reasonable to chose the scattering potential depth so that the calculated direct capture cross section is obtained in the nonresonant regions as far away from the resonances as possible.

IV. CONCLUSIONS AND SUMMARY

The goal of the present work is an investigation of the direct capture method for determining accurate spectroscopic factors. To this end, we have selected reliable cross section data measured in direct proton capture studies and in proton transfer reaction experiments involving $A=16-32$ target nuclei. Spectroscopic factors are reanalyzed and are extracted from the existing data for both types of reactions by using the *same bound state potential parameters*. We also consider the influence of the (direct capture) scattering potential on the value of the derived direct capture spectroscopic factors. The quantitative comparison of C^2S values derived from direct capture experiments to those from DWBA studies and to shell model results represents a sensitive test of the direct capture method.

About half of all previous direct capture studies employed a square-well bound state potential (Table I). In such cases, the published C^2S_{DC} values (column 6 of Table II) for certain levels differ by factors of up to 3 from the present values that are obtained by using a more realistic Woods-Saxon potential (for the same scattering potential; see column 3 of IV). This disagreement has already been pointed out by Powell *et al.* [36] in connection with the $^{24}Mg(p,\gamma)^{25}Al$ reaction. We find deviations of similar magnitude for other reactions as well.

The majority of previous direct capture studies employed hard-sphere scattering potentials (Table I) and thus have treated direct capture strictly as an extranuclear process. We extract C^2S_{DC} values for four different choices of scattering potentials (columns 3–6 of Table IV). The poorest agreement between direct capture and proton transfer spectroscopic factors is found if the same potential is used for calculating the bound state and scattering state radial wave functions. The disagreement reflects the fact that for this particular choice of scattering potential the calculated capture cross section may exhibit in some cases a resonant behavior. The best agreement between C^2S_{DC} and C^2S_{DWBA} values (within about 15% on average) is found for scattering potentials that correspond to the inflection points between resonances of the S factor versus potential depth curve (for example, see Fig. 2). The S factor at these points is equal to the one obtained with a zero scattering potential. We conclude that the direct capture method provides spectroscopic factors of similar accuracy as the transfer reaction method (say, with an error of about 25%; see Sec. I) if the calculated direct capture cross section is obtained using a zero scattering potential (i.e., by taking some capture contributions from inside, and close to, the nuclear radius into account) instead of the common choice of a hard-sphere scattering potential.

ACKNOWLEDGMENTS

This work was supported in part by the U.S. Department of Energy under Grant No. DE-FG02-97ER41041 and by the Joint Institute for Nuclear Astrophysics (JINA) under Grant No. PHY-02-16783.

APPENDIX

In the following, we explain in more detail why certain levels have been disregarded in the present analysis.

A. $^{20}Ne+p$ and $^{22}Ne+p$

Reliable proton stripping cross sections have been measured in studies of the $^{20}Ne(d,n)^{21}Na$ and $^{22}Ne(^3He,d)^{23}Na$ reactions [37,38]. Experimental direct capture cross sections have been reported by Rolfs *et al.* [9] and Görres *et al.* [11]. All cross sections for the $^{20}Ne(p,\gamma)^{21}Na$ and $^{22}Ne(p,\gamma)^{23}Na$ reactions reported by Refs. [9,11] are normalized relative to the direct capture cross section of the $DC\rightarrow 2425$ keV transition in $^{20}Ne(p,\gamma)^{21}Na$ [9]. There is recent evidence that the measured absolute cross section for this transition has been overestimated by a factor of 1.5 or more [39]. Since the issue is currently not resolved yet, we have excluded ^{21}Na and ^{23}Na levels from the present analysis.

B. $^{28}Si+p$

Direct capture transitions to the ground state and to the first excited state ($E_x=1384$ keV) in ^{29}P have been reported by Refs. [12,16].

For the direct capture transition to the first excited state, the γ-ray angular distribution is isotropic (see Fig. 4 of Ref. [12]). From the differential direct capture cross section shown in Fig. 4 of Ref. [16], we obtain at $E_p=1.5$ MeV a total cross section of $\sigma_{DC,exp}=0.11$ μb ($\pm 15\%$). This value disagrees with the value $\sigma_{DC,exp}=0.042$ μb ($\pm 15\%$), reported in Fig. 3 of Ref. [12].

For the direct capture transition to the ground state, we obtain from the differential cross section at $\theta=90°$, shown in Fig. 3 of Ref. [16], a total direct capture cross section of $\sigma_{DC,exp}=0.23$ μb ($\pm 25\%$) [$W(90°)=1.5$] at $E_p=1.5$ MeV. This result agrees with the value $\sigma_{DC,exp}=0.22$ μb ($\pm 14\%$) obtained from Fig. 2 of Ref. [12].

The excitation functions published in Terrasi *et al.* [16] and Graff *et al.* [12], for both the transitions to the ground and first excited state, are dominated by three broad resonances over the entire bombarding energy range. In fact, of all the reactions listed in Table I the relative contribution of the direct capture process is by far the smallest for the $^{28}Si+p$ reaction. As a result, we expect that the extraction of spectroscopic factors from the data is less reliable for this reaction. Consequently, we have disregarded both transitions in the present analysis.

C. $^{40}Ca+p$

Direct capture transitions to the ground state and to the first excited state ($E_x=1716$ keV) in ^{41}Sc have been reported by Ref. [17]. Of those two levels, only the ground state is

bound ($Q_{p\gamma}$=1085 keV). The count rate in the bombarding energy range E_p=2.1–3.1 MeV was rather small and, therefore, the measured excitation function is not sufficiently reliable to extract a spectroscopic factor. The cross section for direct capture to the ground state, displayed in Fig. 2 of Ref. [17], was obtained by *assuming* a value of $C^2S=1$. We have disregarded this transition in the present analysis since the statistics of the published cross section is poor.

[1] P. J. Brussaard and P. W. Glaudemans, *Shell-Model Applications in Nuclear Spectroscopy* (North-Holland, Amsterdam, 1977).
[2] C. Iliadis, J. M. D'Auria, S. Starrfield, W. J. Thompson, and M. Wiescher, Astrophys. J., Suppl. Ser. **134**, 151 (2001).
[3] N. K. Glendenning, *Direct Nuclear Reactions* (Academic, New York, 1983).
[4] J. Vernotte, G. Berrier-Ronsin, J. Kalifa, R. Tamisier, and B. H. Wildenthal, Nucl. Phys. **A571**, 1 (1994).
[5] P. M. Endt, At. Data Nucl. Data Tables **19**, 23 (1977).
[6] C. Rolfs, Nucl. Phys. **A217**, 29 (1973).
[7] C. Rolfs and R. E. Azuma, Nucl. Phys. **A227**, 291 (1974).
[8] H. P. Trautvetter and C. Rolfs, Nucl. Phys. **A242**, 519 (1975).
[9] C. Rolfs, W. S. Rodney, M. H. Shapiro, and H. Winkler, Nucl. Phys. **A241**, 460 (1975).
[10] M. Wiescher, H. W. Becker, J. Görres, K. U. Kettner, H. P. Trautvetter, W. E. Kieser, C. Rolfs, R. E. Azuma, K. P. Jackson, and J. W. Hammer, Nucl. Phys. **A349**, 165 (1980).
[11] J. Görres, H. W. Becker, L. Buchmann, C. Rolfs, P. Schmalbrock, H. P. Trautvetter, A. Vlieks, J. W. Hammer, and T. R. Donoghue, Nucl. Phys. **A408**, 372 (1983).
[12] S. Graff, J. Görres, M. Wiescher, R. E. Azuma, J. King, J. Vise, G. Hardie, and T. R. Wang, Nucl. Phys. **A510**, 346 (1990).
[13] C. Iliadis, U. Giesen, J. Görres, M. Wiescher, S. M. Graff, R. E. Azuma, and C. A. Barnes, Nucl. Phys. **A539**, 97 (1992).
[14] A. M. Mukhamedzhanov, C. A. Gagliardi, and R. E. Tribble, Phys. Rev. C **63**, 024612 (2001).
[15] P. F. Bertone, A. E. Champagne, M. Boswell, C. Iliadis, S. E. Hale, V. Y. Hansper, and D. C. Powell, Phys. Rev. C **66**, 055804 (2002).
[16] F. Terrasi, A. Brondi, P. Cuzzocrea, R. Moro, and M. Romano, Nucl. Phys. **A324**, 1 (1979).
[17] F. Terrasi, A. Brondi, P. Cuzzocrea, R. Moro, G. La Rana, M. Romano, B. Gonsior, N. Notthoff, and E. Kabuss, Nucl. Phys. **A394**, 405 (1983).
[18] A. M. Lane and R. G. Thomas, Rev. Mod. Phys. **30**, 257 (1958).
[19] A. Csoto, Phys. Rev. C **61**, 037601 (2000).
[20] J. Escher, B. K. Jennings, and H. S. Sherif, Phys. Rev. C **64**, 065801 (2001).
[21] G. Hardie, R. E. Segel, A. J. Elwyn, and J. E. Monahan, Phys. Rev. C **38**, 2003 (1988).
[22] H. C. Chow, G. M. Griffiths, and T. H. Hall, Can. J. Phys. **53**, 1672 (1975).
[23] D. Baye and P. Descouvemont, Ann. Phys. (N.Y.) **165**, 115 (1985).
[24] C. Angulo *et al.*, Nucl. Phys. **A656**, 3 (1999).
[25] J. H. Kelley, R. S. Canon, S. J. Gaff, R. M. Prior, B. J. Rice, E. C. Schreiber, M. Spraker, D. R. Tilley, E. A. Wulf, and H. R. Weller, Phys. Rev. C **62**, 025803 (2000).
[26] C. M. Perey and F. G. Perey, At. Data Nucl. Data Tables **17**, 1 (1976).
[27] R. H. Bassel, Phys. Rev. **149**, 791 (1966).
[28] P. D. Kunz, program DWUCK4, extended version of J. R. Comfort.
[29] V. Landre, P. Aguer, G. Bogaert, A. Lefebvre, J. P. Thibaud, S. Fortier, J. M. Maison, and J. Vernotte, Phys. Rev. C **40**, 1972 (1989).
[30] L. M. Polsky, C. H. Holbrow, and R. Middleton, Phys. Rev. **186**, 966 (1969).
[31] E. C. Halbert, J. B. McGrory, B. H. Wildenthal, and S. P. Pandya, in *Advances in Nuclear Physics 4*, edited by M. Baranger and E. Vogt (Plenum, New York, 1971).
[32] B. H. Wildenthal, Prog. Part. Nucl. Phys. **11**, 5 (1984).
[33] T. T. S. Kuo, Nucl. Phys. **A103**, 71 (1967).
[34] P. Möller and J. Randrup, Nucl. Phys. **A514**, 1 (1990).
[35] C. Iliadis, P. M. Endt, N. Prantzos, and W. J. Thompson, Astrophys. J. **524**, 434 (1999).
[36] D. C. Powell, C. Iliadis, A. E. Champagne, C. A. Grossmann, S. E. Hale, V. Y. Hansper, and L. K. McLean, Nucl. Phys. **A660**, 349 (1999)
[37] A. Terakawa, T. Tohei, T. Nakagawa, A. Sato, J. Takamatsu, M. Mori, A. Narita, H. Orihara, K. Ishii, T. Niizeki, M. Oura, S. Hirasaki, M. Hosaka, G. C. Jon, K. Miura, and H. Ohnuma, Phys. Rev. C **48**, 2775 (1993).
[38] J. R. Powers, H. T. Fortune, R. Middleton, and O. Hansen, Phys. Rev. C **4**, 2030 (1971).
[39] E. Stech, Ph.D. thesis, University of Notre Dame, 2004.
[40] P. M. Endt, Nucl. Phys. **A521**, 1 (1990).
[41] P. M. Endt, Nucl. Phys. **A633**, 1 (1998).
[42] D. R. Tilley, H. R. Weller, C. M. Cheves, and R. M. Chasteler, Nucl. Phys. **A595**, 1 (1995).
[43] C. Iliadis, Ph.D. thesis, University of Notre Dame, 1993.